

Using the Spatial Distribution of Automatically Detected Impact Crater's as a Tool to Map the Lunar Surface at High-resolution.

J. H. Fairweather¹, A. Lagain¹, K. Servis^{1,2}, G.K. Benedix^{1,3,4}, S.S. Kumar⁵, and P.A. Bland^{1,3}. ¹School of Earth and Planetary Sciences, Curtin University, GPO Box U1987, Perth, WA, 6845, Australia. ²CSIRO, Pawsey Supercomputing Centre, Kensington, WA, 6151, Australia. ³Department of Earth and Planetary Sciences, Western Australia Museum, Locked Bag 49, Welshpool, WA 6986, Australia. ⁴Planetary Science Institute, 1700 East Fort Lowell, Suite 106, Tuscon AZ 85719-2395, USA. ⁵Department of Geology and Geophysics Indian Institute of Technology Kharagpur, India. (john.fairweather@postgrad.curtin.edu.au).

Introduction: The Moon has been extensively studied over the centuries and with growing technological advances we are able to gather never before seen detail of the Moon's surface, composition, and surface age. Impact craters constellating the lunar surface are the most abundant geological feature and have been used as a tool to map and date the geological events that have shaped the surface.

Over the last 60 years, researchers have used impact crater densities as a quantitative method to compute model ages of the surface [1]. This method works on the premise that differing crater densities indicate relative ages of the surface; the more craters, the older the surface. Crater counting becomes an absolute chronometer when calibrated through the radiometric ages of collected lunar samples. The continued use of this method is dependent on the ability to count and accurately measure the size of impact craters. This is made possible through the vast amount of high-resolution imagery (e.g. Narrow-Angle Camera, NAC images at 0.5-2m/px) via the Lunar Reconnaissance Orbiter Camera (LROC) [2].

On the Moon, craters smaller than 1km in diameter number in the tens of millions. Crater density in this size range, on a particular geological unit, is dependent on the age of the surface, subsequent resurfacing processes, erosion, potential contamination of secondary craters, and the rheology of the surface [3]. It has been shown that the latter parameter affects the final size of an impact crater for a constant impactor size [3]. Thus, the analysis of the spatial distribution of small impact craters across the lunar surface constitutes a powerful tool to derive model ages of the surface and its physical properties. However, as impact crater frequencies evolves as a power law, the ability to count and measure smaller craters in a timely manner is limited to small areas when using a manual counting method.

In previous studies [4,5], we presented the development and subsequent improvement of a Crater Detection Algorithm (CDA), which uses a Convolutional Neural Network (CNN) to detect craters on georeferenced Martian images capable of delivering meaningful surface model ages. One advantage in automating crater detections is the reproducibility of the

results and limiting the variability of crater counts compared to hand-marked crater identification [6].

Adapting the network to the detection of lunar impact craters down to 15m in diameter using LROC-NAC images would therefore provide an invaluable tool to map and date the surface at an ultimate resolution.

Method: The CDA is a machine-learning-based Convolutional Neural Network (CNN) using You Only Look Once version 3 (YOLOv3) as its architecture [7], originally trained on the detection of Martian impact craters on different imagery dataset [4,5]. For the purpose of our study, a retraining of the network is necessary to achieve acceptable recall and precision as well as estimation of crater size.

To train the CDA, we prepared a dataset of 188 tiled NAC images (416x416 pixels) covering two major lunar terrains (mare and highlands). The training dataset consists of 25,973 manually marked craters using Yolo_Mark [8]. To ensure consistent results, all the training images have incidence angles ranging from 65-75° (afternoon/morning lighting) which produces favourable shadows when identifying impact structures.

The training dataset was then augmented by applying a range of transformations (rotate, shear, scale, and translate) using YOLOv3; using 75% of the image tiles for training, and keeping the remaining 25% for validation. Once the pre-determined amount of training iterations was complete, the obtained model was applied to the georeferenced image dataset.

The first step of lunar image georeferencing is done through the US Geological Survey's Integrated Software for Imagers and Spectrometers v3 (ISIS3) [9], then converted into the correct GeoTiff format using GDAL scripts. The GeoTiff image was broken up into tiles (416x416 pixels) and the CDA was run on each tile. The algorithm then combines all detections into a single file containing detection coordinates and size. From raw images to detected impact craters, the processing of thousands of single, or mosaicked, NAC images may take up to a day to get millions of detections using high-performance computing.

Model evaluation: We applied the trained CDA to two NAC images covering both highland and mare surfaces (M1320016983L & M1338833866L). To evaluate the model we manually mapped impact craters larger than 5m in diameter across a 1.5km² subsection of the NAC images, resulting in 3165 craters. This crater population was used to evaluate the accuracy of the model in terms of true-positive (TP), false-negative (FN), and false-positive (FP) detection rates, but also the precision in the diameter estimation of the true positive detections (Table 1). We found that our model produces excellent detection rates (TP>80%) for D>15m (~15px in diameter) and the error in the detection diameter is less than 10% of the manual counterpart (Table 1). For craters larger than 100m in diameter, we also evaluated the accuracy of the model based on their crater degradation state. Very degraded, rimless, impact craters (bottom 3 lines on Table 1) are poorly detected by the CDA (TP<50%), while detection rates and errors associated with fresh or intermediate degradation state craters are acceptable.

Conclusions: Detections obtained through the CDA can be used as a mapping tool to visualise the spatial variations of crater densities, thus allowing to discern structural boundaries of geological units. This includes the identification of high-density areas of small craters (Figure 1), which is potentially from a secondary origin. While low cratering density could indicate recent geological activity, potential deviation from the theoretical production function due to the regolith thickness, or other physical properties of the impacted surface. Overall, the ability to detect 1000s of small craters accurately and quickly gives the CDA unparalleled detail in fine-scale mapping of the lunar surface.

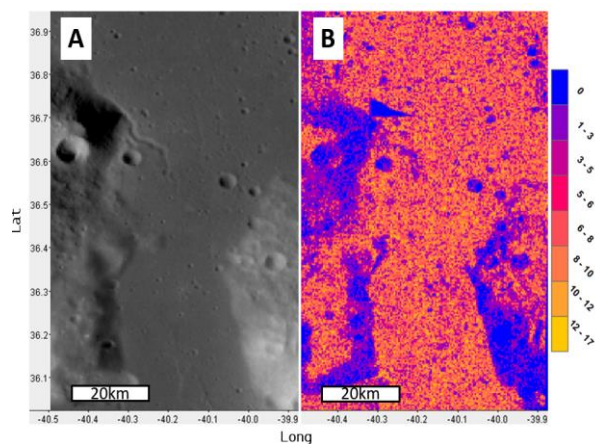

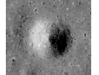



Figure 1: A) Subsection of a LROC-WAC image of the Gruithuisen Domes (NAC_ROI_GRUITHSNLOA); B) impact crater density map made using CDA detection (124,312 craters), legend displays the impact crater density per pixel (note: each pixel is 0.05 of a degree).

Table 1: Confusion matrix comparing the CDA detection against manually mapped craters across different diameter range and degradation state over a Highland terrain (M1338833866L). Note: positive (+) diameter estimations indicate the CDA overestimated the diameter, while negative (-) indicates an underestimation. '*' = TP/FN/FP rates are not representative, due to very small sample sizes ($n < 10$).

Deg. type	Crater Diameter	TP %	FN %	FP %	Manual detections	CDA detections	Av. Diameter estimation ($\pm 2\sigma$)
All	$\geq 5m$	69.4	30.6	6.1	3165	2340	+18.9% (± 25.2)
	$\geq 15m$	83.8	16.2	21.5	74	79	+6.75% (± 27.0)
	$\geq 20m$	86.0	14.0	7.5	43	40	+3.92% (± 11.2)
	$\geq 25m$	90.0	10.0	6.9	30	29	+4.53% (± 22.3)
	$\geq 50m$	*75.0	*25	*0.0	8	6	-2.48% (± 23.4)
	$\geq 100m$	97.1	2.9	-	34	33	+9.9 (± 17.6)
	$\geq 250m$	91.6	8.4	-	12	11	+10.7% (± 9.1)
	$\geq 500m$	*100.0	*0.0	-	4	4	-8.9% (± 44.9)
	$\geq 100m$	80.1	19.9	-	42	34	+7.5% (± 34.3)
	$\geq 250m$	93.3	6.7	-	15	14	+11.2% (± 16.9)
	$\geq 500m$	*66.6	*33.4	-	3	2	+0.4% (± 32.3)
	$\geq 100m$	41.5	58.5	-	53	22	-5.5% (± 30.2)
	$\geq 250m$	38.5	61.5	-	26	10	+9.4% (± 18.8)
	$\geq 500m$	*50.0	*50.0	-	6	3	+10.2% (± 4.3)

Acknowledgments: This work is supported by the resources provided by the Pawsey Supercomputing Centre with funding from the Australian Government, Curtin University, and the Government of Western Australia.

References: [1] Neukum G., Ivanov B. and Hartmann, W.K. (2001). Chronology and Evolution of Mars, Sp. Sci. Rev. 96, 55–86. [2] Robinson, M.S., et al. (2010). Sp. Sci. Rev. 150, 81-124. [3] van der Bogert, C.H., et al. (2017). Icarus. 298, 49-63. [4] Lagain, A., et al. (2021). Earth and Space Science. <https://doi.org/10.1029/2020EA001598>. [5] Benedix, G.K., et al. (2020). Earth and Space Science. <https://doi.org/10.1029/2019EA001005>. [6] Robbins, S.J., et al. (2014). Icarus. 234, 109–131. [7] Redmon, J., Farhadi, A. (2018). arXiv :1804.02767. [8] https://github.com/AlexeyAB/Yolo_mark. [9] <https://isis.astrogeology.usgs.gov/>.